Contemporary Mathematics
https://ojs.wiserpub.com/index.php/CM/

Research Article

Numerical Investigation of Solitary Wave Behavior of Certain Types of Nonlinear Partial Differential Equations

Shumoua F. Alrzqi[1], Fatimah A. Alrawajeh[1], Hany N. Hassan[2*]

[1]Department of Mathematics, College of Science, Imam Abdulrahman Bin Faisal University, Dammam, Eastern Province, P.O. Box 1982, Saudi Arabia
[2]Department of Basic Sciences, Deanship of Preparatory Year and Supporting Studies, Imam Abdulrahman Bin Faisal University, Dammam, Eastern Province, P.O. Box 1982, Saudi Arabia
E-mail: hngomaa@iau.edu.sa

Received: 17 October 2025; **Revised:** 30 October 2025; **Accepted:** 4 January 2026

Abstract: The objective of this work is to obtain accurate numerical results of certain types of partial differential equations with boundary conditions by integrating the Fourier Spectral Method (FSM) for spatial discretization and the Central Finite Difference Method (CFDM) for time integration. The novelty of this study lies in this combination, which enhances accuracy and stability for solving nonlinear dispersive shallow water wave equations while preserving physical invariants such as momentum and energy. Five distinct applications are solved, each representing solitary wave phenomena. The accuracy and efficiency of the used method are measured through evaluating the error norms and conservation properties. To demonstrate the potency and nature of the raised solutions, the 2D and 3D graphical representations and the tables are introduced, showing that the proposed approach achieves high numerical precision and successfully reproduces the physical behavior of solitary waves, preserving their amplitude and energy during propagation.

***Keywords*:** modified Fornberg-Whitham (mFW), modified Degasperis-Procesi (mDP), modified Camassa-Holm (mCH), Korteweg-de Vries-Benjamin-Bona-Mahony-Burgers (KdV-BBM-B), Generalized Rosenau-Regularized Long Wave (GN-R-RLW), solitary waves, finite difference, Fourier Spectral Method (FSM)

MSC: 35C07, 35B10, 65A05, 65M06, 65T50

1. Introduction

Nonlinear Wave Equations (NLWEs) are fundamental models that arise in various scientific disciplines, particularly in physics, where they describe complex wave phenomena and nonlinear dynamics. Due to their wide range of applications across fluid mechanics, plasma dynamics, and nonlinear optics, the study of NLWEs and their solutions has remained the main area of research [1–3]. Among these equations are the modified Fornberg-Whitham (mFW), modified Degasperis-Procesi (mDP), modified Camassa-Holm (mCH), Korteweg-de Vries-Benjamin-Bona-Mahony-Burgers (KdV-BBM-B), and Generalized Rosenau-Regularized Long Wave (GN-R-RLW) equations, which are essential for understanding challenging nonlinear wave phenomena. Whitham first introduced the Fornberg-Whitham equation in his work on wave behavior. This equation admits traveling wave solutions, including kink-like and anti-kink-like forms. Subsequently, in [4], the mFW equation was investigated and expressed the mFW equation as follows

DOI: https://doi.org/10.37256/cm.7220268930

$$u_t - u_{xxt} + u_x + u^2 u_x - u u_{xxx} - 3u_x u_{xx} = 0. \tag{1}$$

The mFW equation demonstrates peakon structures, capturing essential features of nonlinear shallow water wave dynamics. About 71% of Earth's surface is ocean, where absorbed solar radiation drives temperature gradients that generate wind waves propagating long distances before reaching shorelines [5, 6]. In 1993, Camassa and Holm developed a completely integrable model describing unidirectional shallow water wave propagation over a flat bottom. The Camassa-Holm equation models solitons and wave breaking due to nonlinearity and dispersion, however, its applicability is limited in deeper waters. To address this limitation, the mCH equation was proposed and is given by

$$u_t - u_{xxt} + 3u^2 u_x - 2u_x u_{xx} - u u_{xxx} = 0. \tag{2}$$

This modification improves the original model, offering a more accurate representation of soliton interactions and nonlinear dispersive effects [7]. Following these developments, Degasperis and Procesi introduced the Degasperis-Procesi (DP) equation in 1999 for two-dimensional water waves over a flat bottom, and later Wazwaz [8] investigated its modified form (mDP), expressed as follows

$$u_t - u_{xxt} + 4u^2 u_x - u u_{xxx} - 3u_x u_{xx} = 0. \tag{3}$$

To model weakly nonlinear, dispersive long wave propagation with dissipation, such as water waves and gas dynamics, the KdV-BBM-B equation was derived by combining the Korteweg-de Vries, Benjamin-Bona-Mahony, and Burgers equations [9]. It is given by

$$u_t + a u_x + b u u_x + d u_{xx} - e u_{xxt} + f u_{xxx} = 0. \tag{4}$$

Extending classical wave models, the GN-R-RLW equation combines components of the generalized Rosenau and regularized long wave equations, enabling analysis of nonlinear structures such as solitons and shock waves [10].

$$u_t + u_{xxxxt} - u_{xxt} + u_x + (u^p)_x = 0. \tag{5}$$

For all the above equations, the initial and boundary conditions are defined respectively, where $u = u(x, t)$ and $F(x)$, $G(t)$, $H(t)$ are known functions [11]. The solution domain is defined over a finite spatial interval $[a, b]$ and a positive time period $t \geq 0$, where $u(x, t)$ represents the wave amplitude or physical variable of interest, x and t denote the spatial and temporal variables. Homogeneous boundary conditions are assumed such that $u \to 0$ as $x \to \pm\infty$.

$$\begin{cases} u(x, 0) = F(x), \quad x \in [a, b], \\ \\ u(a, t) = G(t), \quad u(b, t) = H(t), \quad t > 0. \end{cases} \tag{6}$$

Despite extensive efforts to obtain analytical solutions, the strong nonlinearity of these equations often restricts the possibility of deriving exact results. Consequently, numerical methods have become essential for approximating and analyzing their behavior. Several numerical techniques have been proposed in the literature, including the Haar Wavelet (HW) collocation method [12, 13], finite element and spectral collocation methods [14–21], finite difference schemes [11, 22], the Differential Quadrature Method (DQM) [23], and Fourier pseudo-spectral methods [24–28], operational and operational matrix techniques [29, 30], the Supplementary Variable Method (SVM) [31], the Petrov-Galerkin approach [32, 33], and the reproducing kernel method [34, 35]. And other related techniques. In this study, we focus on the numerical solution of five NLWEs: mFW, mDP, mCH, KdV-BBM-B, and GN-R-RLW. The proposed method combines the Central Finite Difference Method (CFDM) method for time discretization, offering second-order accuracy, and the FSM for spatial discretization using the Fast Fourier Transform (FFT) to handle periodic boundary conditions. Section 2 outlines the methodology, preliminary concepts, and analysis of the numerical scheme; Section 3 presents the numerical experiments and corresponding tabulated and graphical results; and Section 4 summarizes the main findings.

2. Methodology

2.1 *Preliminary*

This section introduces the key mathematical concepts and notations utilized throughout this study. These preliminaries form the foundation for the numerical formulation and analysis. Specifically, two conserved quantities relevant to shallow water wave dynamics are defined: the momentum I_M and the energy I_E. These invariants are evaluated during the solitary wave simulations to assess the accuracy and efficiency of the proposed numerical method by comparing numerical and analytical results.

Definition 1 Let $\Omega = [a, b]$ be a bounded domain, and let $u^{(q)}$ denote the q-th order derivative. Then the Sobolev spaces $H^2(\Omega)$ and $H_0^2(\Omega)$ are defined as follows

$$H^2(\Omega) = \left\{ u: \int_\Omega \left(u^{(q)}\right)^2 dx < \infty,\ q = 0, 1, 2 \right\}, \tag{7}$$

$$H_0^2(\Omega) = \left\{ u: u \in H^2(\Omega),\ \frac{\partial^i u}{\partial x^i} = 0 \text{ on } \partial\Omega \quad i = 0, 1, 2 \right\}. \tag{8}$$

Lemma 1 Suppose $u_0 \in H_0^2[a, b]$. Then, the solution satisfies the mass conservation

$$I_M(t) = \int_a^b u(x, t)dx = \int_a^b u(x, 0)dx = \int_a^b u_0 dx = I_M(0).$$

Theorem 1 Suppose that $u_0 \in H_0^2[a, b]$ and $u(x, t)$ represents the solution of the governing equation. Then, the total energy is conserved and given by

$$I_E(t) = \int_a^b \left[u^2(x, t) + eu_x^2(x, t) + cu_{xx}^2(x, t)\right] dx = \|u\|_{L_2}^2 + e\|u_x\|_{L_2}^2 + c\|u_{xx}\|_{L_2}^2 = I_E(0),\ e \geq 0.$$

Theorem 2 If $u_0 \in H_0^2[a, b]$, then the solution satisfies $\|u\|_{L_2} \leq C$, $\|u_x\|_{L_2} \leq C$, $\|u_{xx}\|_{L_2} \leq C$, and, hence $\|u\|_{L_\infty} \leq C$ and $\|u_x\|_{L_\infty} \leq C$.

Theorem 3 If $u_0 \in H_0^2[a, b]$, then the problem under consideration is well-posed.

The L_2, L_∞, the Root Mean Square (RMS), and the order of convergence errors are utilized to evaluate the solution accuracy [36, 37].

$$L_2 = \left\|u^{\text{exact}} - u_N\right\|_2 \simeq \sqrt{h\sum_{j=1}^{N}\left|u_j^{\text{exact}} - (u_N)_j\right|^2}, \tag{9}$$

$$L_\infty = \left\|u^{\text{exact}} - u_N\right\|_\infty \simeq \max_j |u_j^{\text{exact}} - (u_N)_j|, \quad j = 1, 2, \ldots, N-1, \tag{10}$$

$$\text{RMS} = \left(\sum_{j=1}^{N}\frac{(u_j^{\text{exact}} - (u_N)_j)^2}{N}\right)^{1/2}, \tag{11}$$

$$\text{Order of convergence} = \frac{\ln\left[L_\infty(h)/L_\infty(h/2)\right]}{\ln 2}. \tag{12}$$

2.2 *Numerical scheme analysis*

The combination of FFT and CFDM is applied to efficiently solve periodic initial value Partial Differential Equation (PDE) problems. The convergence and stability of the employed technique have been studied in [38–40]. In those studies, numerical experiments with different step sizes (Δx, Δt) showed that smaller discretizations improve accuracy while maintaining the structure of solitary waves. $\Delta x = 0.1$ and $\Delta t = 0.001$ were utilized to ensure stability and consistency in this study. The formulation starts with using the nonlinear PDE defined in Eq. (1), after which the method is extended to similar classes of equations. To ensure compatibility with the suggested numerical scheme, the nonlinear terms must be modified for each case.

First, we rewrite Eq. (1) as follows

$$v_t = -(u_x + u^2 u_x - u u_{xxx} - 3u_x u_{xx}), \tag{13}$$

$$v = u - u_{xx}. \tag{14}$$

Eq. (13) and (14) reformulate Eq. (1) into a simpler system, enhancing numerical stability and improving effective integration through the proposed method. To make computation and evaluation easier, the spatial domain is normalized by using the transformation $x \to \frac{2\pi(x-a)}{L}$, which maps the original interval $L = [a, b]$ to $[0, 2\pi]$. By normalizing the spatial domain and using FFT to handle spatial derivatives, computational efficiency is enhanced. The spatial derivatives that result from the Fourier spectral differentiation property are then determined, and FFT is used to assess the derivatives as follows

$$\frac{\partial^n u}{\partial x^n} = F^{-1}\left\{(ik)^n F(u)\right\}, \quad n = 1, 2, \ldots \tag{15}$$

To operate the discrete Fourier transform and its inverse, the spatial domain is discretized into points $x_j = j\Delta x = \frac{2\pi j}{N}$ where $j = 0, 1, \ldots, N-1$. After that, the solution $u(x, t)$ is converted into discrete Fourier space and its inverse, which are represented by

$$\hat{u}(k,t) = \frac{1}{N}\sum_{j=0}^{N-1} u(x_j,t)e^{-ikx_j}, \quad -\frac{N}{2} \le k \le \frac{N}{2}-1, \tag{16}$$

$$u(x_j,t) = \sum_{k=-N/2}^{N/2-1} \hat{u}(k,t)e^{ikx_j}, \quad 0 \le j \le N-1. \tag{17}$$

For simplicity, Eq. (14) and (13) can be written as follows by applying the Fourier transform to both sides

$$\frac{\partial}{\partial t}\hat{v}(k,t) = -(ik)\hat{u}(k,t) - u^2(ik)\hat{u}(k,t) + u(ik)^3\hat{u}(k,t) + 3(ik)^3\left[\hat{u}(k,t)\right]^2. \tag{18}$$

and

$$\hat{v}(k,t) = \hat{u}(k,t) - (ik)^2\hat{u}(k,t). \tag{19}$$

By applying the previous mathematical transformations into Eq. (19) and (18), respectively, we get

$$v(x_j,t) = u(x_j,t) - (2\pi/L)^2 F^{-1}\{-k^2F(u)\}, \tag{20}$$

and

$$\frac{\partial}{\partial t}v(x_j,t) = -\frac{2\pi}{L}F^{-1}\{ikF(u)\} - \frac{2\pi}{L}u^2(x_j,t)F^{-1}\{ikF(u)\} + \frac{(2\pi)^3}{L^3}u(x_j,t)F^{-1}\{ik^3F(u)\}$$

$$-\frac{3(2\pi)^3}{L^3}F^{-1}\{ik^3\big(F(u)\big)^2\}. \tag{21}$$

Then the Ordinary Differential Equation (ODE) Eq. (21) is transformed into vector form as follows

$$\boldsymbol{v}_t = h(\boldsymbol{u}), \quad \text{where} \quad \boldsymbol{u} = \left[u(x_0,t), u(x_1,t), \ldots, u(x_{N-1},t)\right]^T, \tag{22}$$

The right-hand side of the equation is represented by the function $h(\boldsymbol{u})$, which is a term that can be addressed using standard techniques for first-order differential equations. In this study, we use the CFDM, which has been thoroughly investigated in previous studies, including its efficacy, especially concerning convergence and stability [38]. By simplifying Eq. (18) and applying the CFDM, we get

$$v^{n+1} = v^{n-1} + 2\Delta t\, h(u^n). \tag{23}$$

Since two different initial values are required to use the CFDM, we start with $u(x, 0)$, the process determines the first initial, where $v(x, 0)$ is subsequently obtained.

$$v(x, 0) = F^{-1}\left\{(1 + k^2(2\pi/L)^2)F(u(x, 0))\right\}, \tag{24}$$

To obtain the second initial condition indicated by $v(x, \Delta t)$, we use the Runge-Kutta method (RK4), which is a one-step higher-order technique to solve ODEs that takes the following formula

$$\begin{aligned}
R_1 &= h(u(x, 0), 0\big), \\
R_2 &= h\left(u(x, 0) + \frac{1}{2}\Delta t\, R_1, \frac{1}{2}\Delta t\right), \\
R_3 &= h\left(u(x, 0) + \frac{1}{2}\Delta t\, R_2, \frac{1}{2}\Delta t\right), \\
R_4 &= h\left(u(x, 0) + \Delta t\, R_3, \Delta t\right), \\
v(x, \Delta t) &= v(x, 0) + \frac{\Delta t}{6}(R_1 + 2R_2 + 2R_3 + R_4).
\end{aligned} \tag{25}$$

As an essential step, we enter the determined value of $v(x, \Delta t)$ for any $t = n\Delta t$ as follows

$$u(x, n\Delta t) = F^{-1}(F(v(x, \Delta t))/(1 + k^2(2\pi/L)^2)). \tag{26}$$

Subsequently, the solution $u(x, t)$ is obtained by transforming Eq. (22) into

$$\begin{aligned}
v(x, t + \Delta t) =& v(x, t - \Delta t) \; + \; 2\Delta t\Bigg[- \frac{2\pi}{L}F^{-1}\{ikF(u)\} - \frac{2\pi}{L}u^2(x_j, t)F^{-1}\{ikF(v)\} \\
&+ \frac{(2\pi)^3}{L^3}u(x_j, t)F^{-1}\{ik^3F(u)\} - \frac{3(2\pi)^3}{L^3}F^{-1}\{ik^3\big(F(u)\big)^2\}\Bigg].
\end{aligned} \tag{27}$$

Finally, using the FFT in Python, the approximate solution is obtained, which allows $u(x, t)$ to be evaluated at the final time $t = n\Delta t$, while keeping in mind that the accuracy of the numerical method relies on two initial values, which are required by the CFDM. This approach proposes a numerical framework for addressing NLWEs. In the following section, the accuracy, stability, and conservation performance will be evaluated via various numerical experiments.

3. Numerical experiments

This section presents numerical experiments for five examples of NLWEs by employing the formulations and methodology presented in Section 2. All simulations were performed using the proposed method, which was programmed in Python and displayed in MATLAB. The performance is evaluated using error norms, conservation properties, and convergence rates, and the results are compared to previous studies in order to demonstrate the method's accuracy and effectiveness.

3.1 *Modified Fornberg-Whitham (mFW) equation*

Considering Eq. (1), with the following initial condition, where w represents the wave speed, given by [4]

$$u(x,0) = \frac{3}{4}(\sqrt{15}-5)\,\mathrm{sech}^2(wx), \quad w = \frac{1}{20}\sqrt{(10(5-\sqrt{15}))}. \tag{28}$$

Which is directly derived from the exact solution [4]

$$u(x,t) = \frac{3}{4}(\sqrt{15}-5)\,\mathrm{sech}^2(w(x-(5-\sqrt{15})t)). \tag{29}$$

In this example, we set the spatial and temporal discretization parameters as $\Delta t = 0.001$, $\Delta x = 0.1$ for N = 524,288. The accuracy and effectiveness of the employed numerical method are evaluated through the numerical results displayed in Figure 1 and Tables 1, 2 for time intervals $t = 0.1$ to $t = 1$. At $t = 1$, while maintaining an amplitude of 0.845250. Figure 1 (a) displays the propagation of the solitary wave, highlighting the efficiency and accuracy of the numerical solution over time. The error vector shown in Figure 1 (b), remains minimal throughout the simulation. Additionally, Figure 1 (c) presents a 3D representation of the motion of the solitary wave, which verifies the consistency of the numerical results. These results demonstrate that the method effectively preserved the momentum I_M and energy I_E consistently, while maintaining the amplitude around its initial value. Moreover, Table 1 presents the error norms L_∞ and L_2 for various values of N at $t = 1$, demonstrating the performance of the employed numerical method. The convergence of the approach is demonstrated by the significant decrease in error norms as N increases, while the invariants I_M and I_E remain stable across increasing values of N. Table 2 evaluates error norms at various t times, showing that the error norms L_∞ and L_2, which both maintain extremely small values up to 10^{-7}, and RMS error remains low, with a stable order of convergence. Compared to [11], the employed method exhibits a higher accuracy and significantly lower error norms, which shows its efficiency in solving the equation.

Table 1. Behavior of invariants and error norms at $t = 1$, with $\Delta t = 0.001$, $\Delta x = 0.1$, and varying N values for Example 3.1

N	I_M	I_E	L_∞	L_2	Amplitude	CPU (s)
4,096	-10.068861792083	5.801841606098	2.4076×10^{-5}	8.0112×10^{-5}	0.845248	0.9759
8,192	-10.070091201338	5.802518585226	1.2038×10^{-5}	4.0056×10^{-5}	0.845249	1.8792
16,384	-10.070705905965	5.802857076285	6.0193×10^{-6}	2.0029×10^{-5}	0.845250	3.9681
32,768	-10.071013258278	5.803026322188	3.0104×10^{-6}	1.0016×10^{-5}	0.845250	8.6365
65,536	-10.071166934435	5.803110945233	1.5060×10^{-6}	5.0096×10^{-6}	0.845250	17.0267
131,072	-10.071243772513	5.803153256779	7.5377×10^{-7}	2.5064×10^{-6}	0.845250	39.2521
262,144	-10.071282191553	5.803174412557	3.7767×10^{-7}	1.2548×10^{-6}	0.845250	81.8389
524,288	-10.071301401072	5.803184990448	1.8965×10^{-7}	6.2896×10^{-7}	0.845250	159.6830

Table 2. Behavior of invariants and error norms for $N = 524{,}288$, with $\Delta t = 0.001$, $\Delta x = 0.1$, and varying t values for Example 3.1

t	I_M	I_E	L_∞	L_2	RMS	Order of Convergence	Amplitude
0.1	-10.071301401072	5.803184990500	1.8822×10^{-8}	6.2880×10^{-8}	2.7462×10^{-10}	0.996062	0.845229
0.2	-10.071301401072	5.803184990493	3.7682×10^{-8}	1.2576×10^{-7}	5.4924×10^{-10}	0.995761	0.845248
0.4	-10.071301401072	5.803184990464	7.5501×10^{-8}	2.5153×10^{-7}	1.0985×10^{-9}	0.995221	0.845262
0.6	-10.071301401072	5.803184990431	1.1345×10^{-7}	3.7732×10^{-7}	1.6479×10^{-9}	0.994683	0.845246
0.8	-10.071301401072	5.803184990416	1.5150×10^{-7}	5.0312×10^{-7}	2.1973×10^{-9}	0.994207	0.845207
1	-10.071301401072	5.803184990448	1.8965×10^{-7}	6.2896×10^{-7}	2.7469×10^{-9}	0.993818	0.845250
			Comparison of method in [11]				
0.1	-	-	4.42×10^{-4}	1.90×10^{-4}	-	-	-
0.2	-	-	1.79×10^{-3}	5.68×10^{-4}	-	-	-
0.4	-	-	2.93×10^{-3}	9.87×10^{-4}	-	-	-
0.8	-	-	2.08×10^{-3}	7.63×10^{-4}	-	-	-

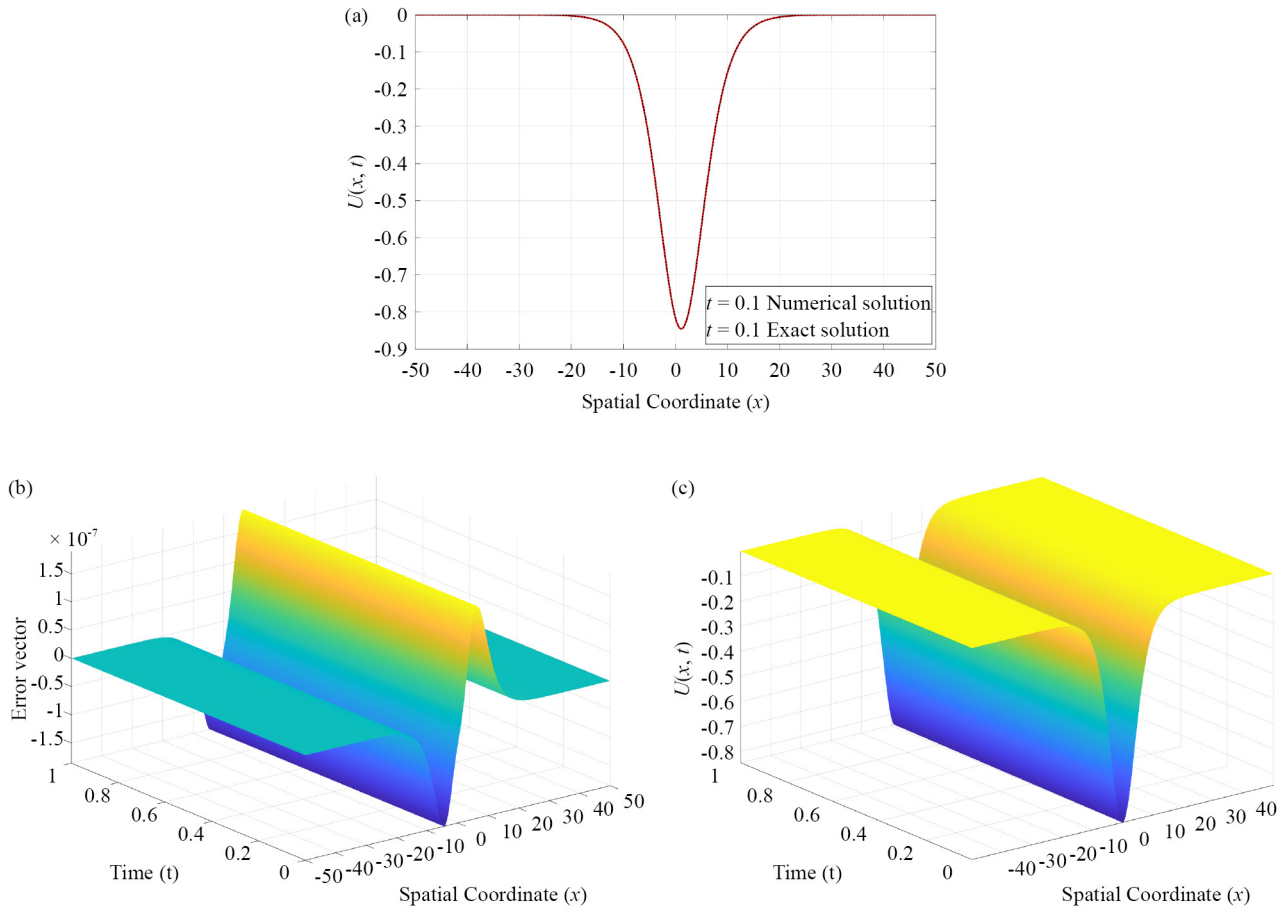

Figure 1. (a) Motion of the solitary wave, (b) Error vector, and (c) 3D representation of the solitary wave motion at $t = 1$, with $N = 524{,}288$, $\Delta t = 0.001$, and $\Delta x = 0.1$ for Example 3.1

3.2 *Modified Camassa-Holm (mCH) equation*

Considering the Eq. (2), with the following initial condition

$$u(x, 0) = -2\,\mathrm{sech}^2\left(\frac{x}{2}\right). \tag{30}$$

With the exact solution [41]

$$u(x, t) = -2\,\mathrm{sech}^2\left(\frac{x}{2} - t\right). \tag{31}$$

Table 3. Behavior of invariants and error norms at $t = 0.75$, with $\Delta t = 0.001$, $\Delta x = 0.1$, and varying N values for Example 3.2

N	I_M	I_E	L_∞	L_2	Amplitude	CPU (s)
4,096	-7.998046875000	12.797903714920	2.1778×10^{-4}	3.6799×10^{-4}	1.998685	0.7047
8,192	-7.999023437500	12.798945286222	1.0851×10^{-4}	1.8344×10^{-4}	1.998717	1.6018
16,384	-7.999511718750	12.799466095726	5.3894×10^{-5}	9.1183×10^{-5}	1.998733	3.1983
32,768	-7.999755859375	12.799726506440	2.6587×10^{-5}	4.5083×10^{-5}	1.998741	6.8921
65,536	-7.999877929688	12.799856713287	1.2960×10^{-5}	2.2086×10^{-5}	1.998745	14.3807
131,072	-7.999938964844	12.799921817083	6.2397×10^{-6}	1.0700×10^{-5}	1.998747	30.7032
262,144	-7.999969482422	12.799954369074	3.0465×10^{-6}	5.2551×10^{-6}	1.998748	66.4174
524,288	-7.999984741210	12.799970645092	1.9645×10^{-6}	3.0191×10^{-6}	1.998749	134.5545

Table 4. Behavior of invariants and error norms for $N = 524{,}288$, with $\Delta t = 0.001$, $\Delta x = 0.1$, and varying t values for Example 3.2

t	I_M	I_E	L_∞	L_2	RMS	Order of Convergence	Amplitude
0.05	-7.999984741210	12.799983560566	2.4177×10^{-7}	3.9139×10^{-7}	1.7094×10^{-9}	0.598739	1.998751
0.10	-7.999984741210	12.799983071856	4.8083×10^{-7}	7.7572×10^{-7}	3.3878×10^{-9}	0.606924	1.998750
0.15	-7.999984741210	12.799982283105	7.1275×10^{-7}	1.1461×10^{-6}	5.0053×10^{-9}	0.622661	1.998750
0.20	-7.999984741210	12.799981235031	9.3504×10^{-7}	1.4961×10^{-6}	6.5340×10^{-9}	0.631236	1.998750
0.25	-7.999984741210	12.799979981584	1.1424×10^{-6}	1.8201×10^{-6}	7.9491×10^{-9}	0.634527	1.998750
0.50	-7.999984741210	12.799973038947	1.9209×10^{-6}	2.9125×10^{-6}	1.2720×10^{-8}	0.586401	1.998749
0.75	-7.999984741210	12.799970645092	1.9645×10^{-6}	3.0191×10^{-6}	1.3185×10^{-8}	0.633016	1.998749

For this example, the motion of a solitary wave is displayed in Figure 2, which shows a comparison between the numerical and the exact solution, along with the error vector, and a 3d representation. Table 3 shows the behavior of conserved quantities I_M and I_E, along with the error norms L_∞ and L_2 at $t = 0.75$ for various values of N. The results demonstrate that the error norms significantly decrease as N increases, while the invariants remain constant, validating the conservation properties of the method. The investigation is expanded in Table 4 by evaluating error norms for $N = 524{,}288$ at various t times. These results confirm that the method has a constant order of convergence and small error

norms. Additionally, the wave amplitude practically stays constant throughout the simulation, which further demonstrates the effectiveness and accuracy of the method.

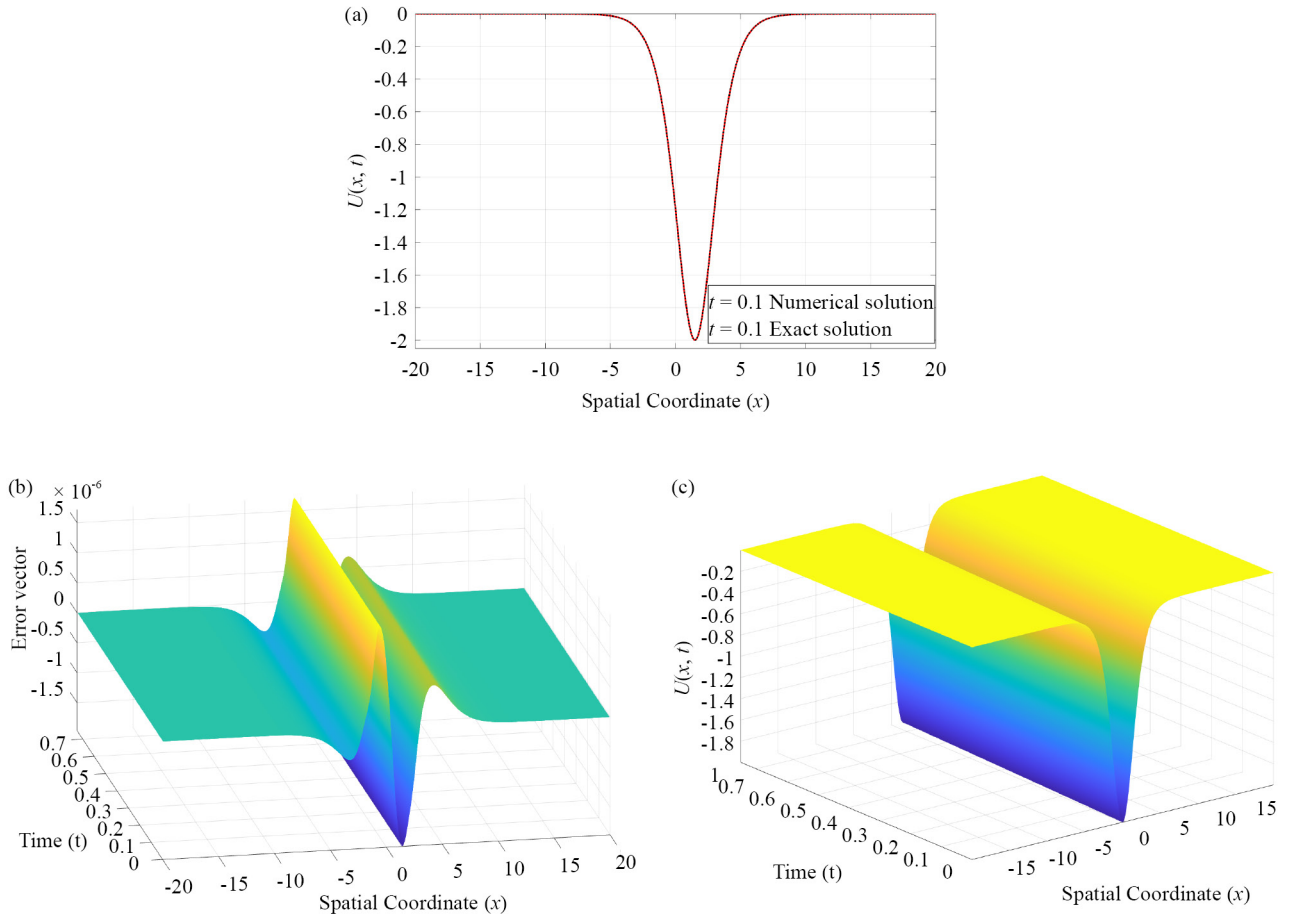

Figure 2. (a) Motion of the solitary wave, (b) Error vector, and (c) 3D representation of the solitary wave motion at $t = 0.75$, with N = 524,288, $\Delta t = 0.001$, and $\Delta x = 0.1$ for Example 3.2

3.3 *Modified Degasperis-Procesi (mDP) equation*

Considering Eq. (3), along with its initial condition and exact solution, respectively [41]

$$u(x, 0) = \frac{-15}{8}\,\mathrm{sech}^2\left(\frac{x}{2}\right). \tag{32}$$

$$u(x, t) = \frac{-15}{8}\,\mathrm{sech}^2\left(\frac{x}{2} - \frac{5t}{4}\right). \tag{33}$$

For this example, the spatial domain x is set as $[-10, 10]$, with a final time of $t = 1$, using $\Delta t = 0.001$ and $\Delta x = 0.1$. The accuracy of the employed method is illustrated by Figure 3, where (a) shows the motion of a single wave, (b) the error vector, and (c) a 3D representation. Table 5 evaluates the invariants I_M and I_E, and the error norms L_∞ and L_2 for various values of N. Those results demonstrate that the conserved properties remain constant, and the wave amplitude is

preserved across all N values. Table 6 extends the behavior of invariants and error norms for N = 524,288 at different time intervals t, demonstrating that the method results maintain stability across all time steps, with consistently low error norms and an order of convergence. Furthermore, the method produces significantly smaller error norms when compared to the Multiquadric (MQ) and Inverse Quadratic (IQ) methods from [11], highlighting its computational accuracy.

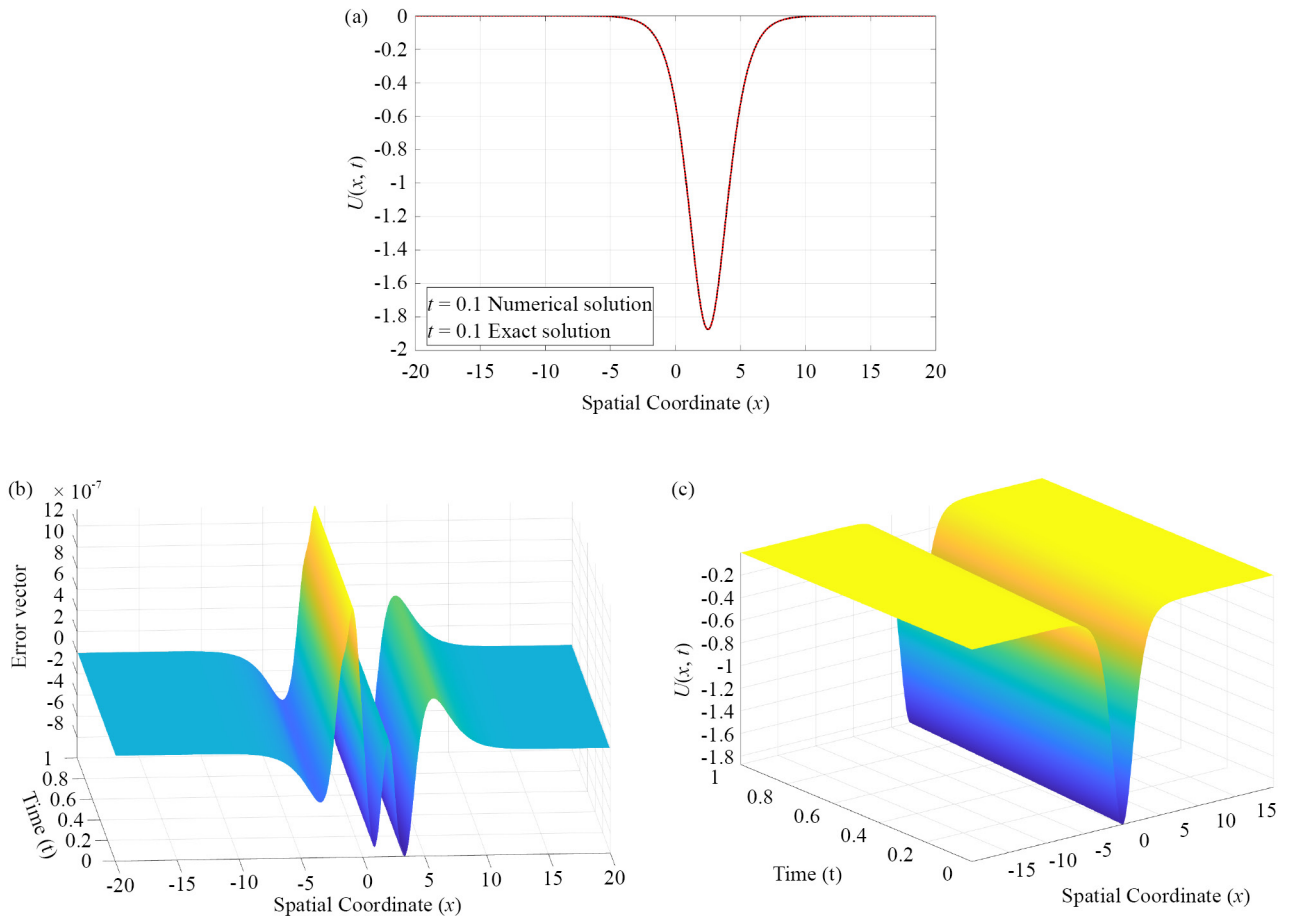

Figure 3. (a) Motion of the solitary wave, (b) Error vector, and (c) 3D representation of the solitary wave motion at $t = 1$, with N = 524,288, $\Delta t = 0.001$, and $\Delta x = 0.1$ for Example 3.3

Table 5. Behavior of invariants and error norms at $t = 1$, with $\Delta t = 0.001$, $\Delta x = 0.1$, and varying N values for Example 3.3

N	I_M	I_E	L_∞	L_2	Amplitude	CPU (s)
4,096	-7.498168945313	11.248424363378	2.5789×10^{-4}	5.0545×10^{-4}	1.873761	0.9038
8,192	-7.499084472656	11.249207845387	1.2755×10^{-4}	2.5054×10^{-4}	1.873795	1.9706
16,384	-7.499542236328	11.249599637890	6.2404×10^{-5}	1.2311×10^{-4}	1.873812	3.9900
32,768	-7.499771118164	11.249795547012	2.9833×10^{-5}	5.9410×10^{-5}	1.873821	8.5480
65,536	-7.499885559082	11.249893504789	1.3548×10^{-5}	2.7594×10^{-5}	1.873825	17.6521
131,072	-7.499942779541	11.249942484482	5.4724×10^{-6}	1.1777×10^{-5}	1.873827	39.9229
262,144	-7.499971389771	11.249966974530	1.8052×10^{-6}	4.1992×10^{-6}	1.873828	86.1501
524,288	-7.499985694885	11.249979219603	1.3560×10^{-6}	2.1634×10^{-6}	1.873829	166.0609

Table 6. Behavior of invariants and error norms for $N = 524{,}288$, with $\Delta t = 0.001$, $\Delta x = 0.1$, and varying t values for Example 3.3

t	I_M	I_E	L_∞	L_2	RMS	Order of Convergence	Amplitude
0.05	-7.499985694885	11.249985251625	4.2746×10^{-7}	7.0364×10^{-7}	3.0730×10^{-9}	0.321469	1.874707
0.1	-7.499985694885	11.249983941381	8.5737×10^{-7}	1.3849×10^{-6}	6.0482×10^{-9}	0.316439	1.875000
0.15	-7.499985694885	11.249981881947	1.2759×10^{-6}	2.0227×10^{-6}	8.8337×10^{-9}	0.313005	1.874706
0.2	-7.499985694885	11.249979257785	1.6718×10^{-6}	2.5989×10^{-6}	1.1350×10^{-8}	0.304995	1.873828
1	-7.499985694885	11.249979219603	1.3560×10^{-6}	2.1634×10^{-6}	9.4482×10^{-9}	0.412827	1.873829
			Comparison of MQ method in [11]				
0.05	-7.499	-	1.42×10^{-4}	1.76×10^{-5}	-	-	-
0.1	-7.499	-	2.64×10^{-4}	1.32×10^{-5}	-	-	-
0.15	-7.499	-	4.11×10^{-4}	7.99×10^{-6}	-	-	-
0.2	-7.499	-	5.82×10^{-4}	4.33×10^{-6}	-	-	-
0.5	-7.499	-	1.33×10^{-3}	2.99×10^{-5}	-	-	-
1	-7.497	-	2.54×10^{-3}	4.53×10^{-5}	-	-	-
			Comparison of IQ method in [11]				
0.05	-7.499	-	1.43×10^{-4}	2.35×10^{-5}	-	-	-
0.1	-7.499	-	2.65×10^{-4}	2.99×10^{-5}	-	-	-
0.15	-7.499	-	4.08×10^{-4}	9.72×10^{-5}	-	-	-
0.2	-7.499	-	5.78×10^{-4}	1.53×10^{-4}	-	-	-
0.5	-7.499	-	1.33×10^{-3}	6.36×10^{-5}	-	-	-
1	-7.497	-	2.54×10^{-3}	8.44×10^{-5}	-	-	-

3.4 *Korteweg-de Vries-Benjamin-Bona-Mahony-Burgers (KdV-BBM-B) equation*

Considering Eq. (4), where $a = b = e = 1$ and $d = f = 0$, with initial condition

$$u(x, 0) = 3c\,\mathrm{sech}^2 k(x), \quad k = \frac{1}{2}\sqrt{\frac{c}{v}}, \quad v = 1 + c. \tag{34}$$

Given the exact solution as [15]

$$u(x, t) = 3c\,\mathrm{sech}^2 k(x - vt). \tag{35}$$

For this example, consider two values of the parameter c, particularly $c = 0.1$ and $c = 0.03$, to evaluate the employed method. The wave motion, error vectors, and 3D representations for both cases are shown in Figure 4. Figures 4 (a)-(c) shows the results for $c = 0.1$, while Figures 4 (d)-(f) shows the results $c = 0.03$. The behavior of invariants and error norms at $t = 20$ for $c = 0.1$ is shown in Table 7. The results validate the method's convergence by showing that the error norms L_∞ and L_2 decrease significantly as N increases. Moreover, the employed method consistently achieves lower error

norms than those presented in [9, 15, 42]. Table 8 extends the examination to various t times and expands the behavior to $c = 0.03$. The results show that the method achieves significantly lower error norms, particularly when N increases, which highlights the robustness and precision of the employed method.

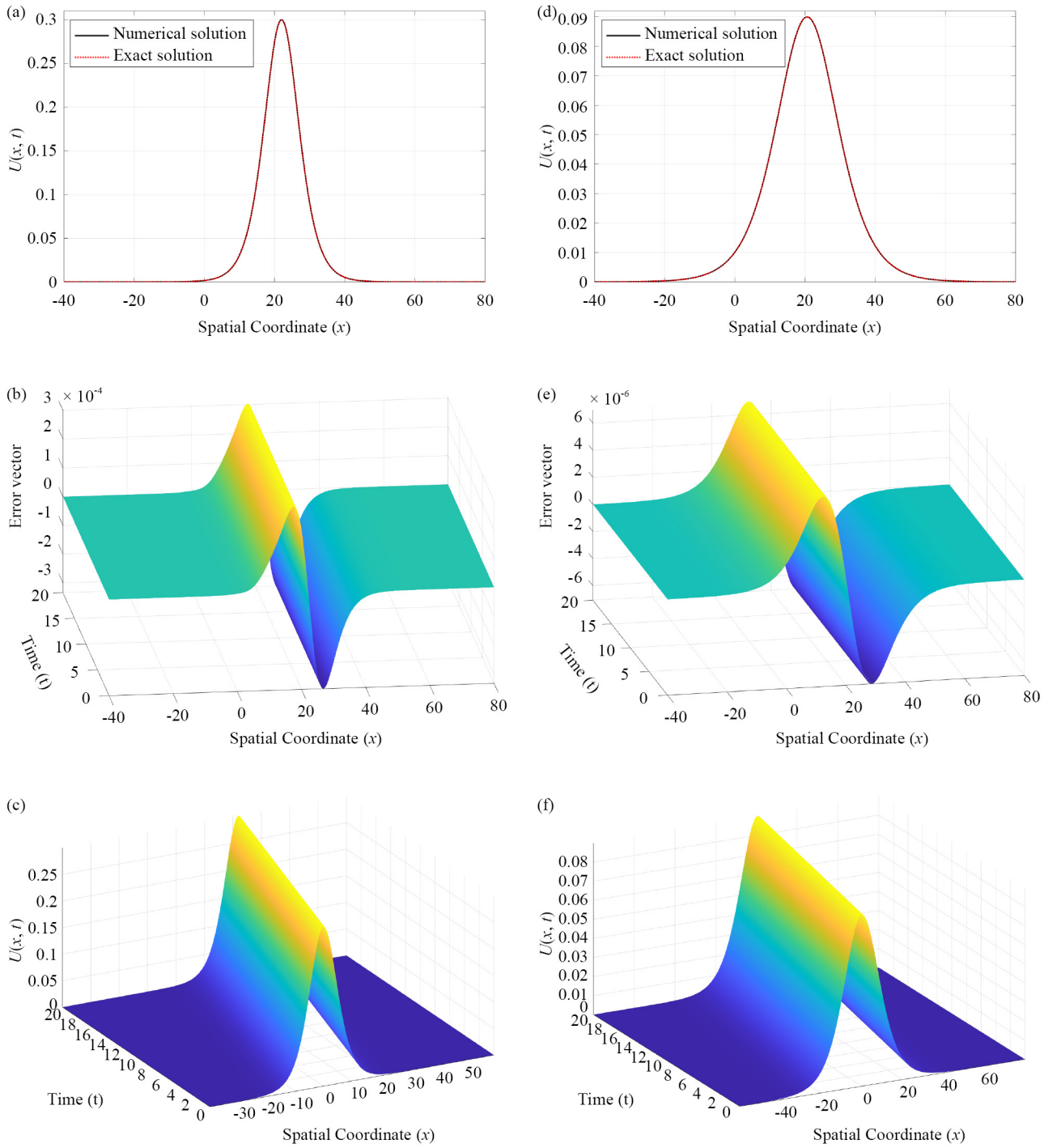

Figure 4. Visualization of the wave motion in Example 3.4 at $t = 20$, with $N = 16{,}384$, $\Delta t = 0.001$, and $\Delta x = 0.1$, for different values of c. subfigures (a), (b), and (c) correspond to $c = 0.1$ and show the motion, error vector, and 3D representation, respectively. subfigures (d), (e), and (f) correspond to $c = 0.03$ and show the motion, error vector, and 3D representation, respectively

Table 7. Behavior of invariants and error norms at $t = 20$, with $c = 0.1$, $\Delta t = 0.001$, $\Delta x = 0.1$, and varying N values for Example 3.4

N	I_M	I_E	L_∞	L_2	Amplitude	CPU (s)
4,096	3.978978081007	0.810271694298	1.6681×10^{-4}	5.7697×10^{-4}	0.299974	18.4562
8,192	3.979463914717	0.810367093726	8.3404×10^{-5}	2.8849×10^{-4}	0.299978	38.3205
16,384	3.979706831572	0.810414793601	4.1704×10^{-5}	1.4426×10^{-4}	0.299981	81.5306
32,768	3.979828289999	0.810438643579	2.0856×10^{-5}	7.2142×10^{-5}	0.299982	193.1568
65,536	3.979889019213	0.810450568578	1.0432×10^{-5}	3.6086×10^{-5}	0.299982	412.3739
131,072	3.979919383820	0.810456531081	5.2201×10^{-6}	1.8058×10^{-5}	0.299983	925.6300
262,144	3.979934566123	0.810459512332	2.6141×10^{-6}	9.0440×10^{-6}	0.299983	2076.6573
524,288	3.979942157275	0.810461002958	1.3111×10^{-6}	4.5371×10^{-6}	0.299983	4659.6674
Comparative study with other methods at $t = 20$						
RBF-PS [9]	3.9760436	0.80965203	1.2668×10^{-5}	2.8004×10^{-5}	-	-
RBF-FD [9]	3.9760436	0.80965203	1.2668×10^{-5}	2.8004×10^{-5}	-	-
[15]	3.9798820	0.8104627	8.4558×10^{-5}	2.1615×10^{-4}	-	-
[42]	3.97993	0.810462	1.4977×10^{-5}	4.7573×10^{-5}	-	-

Table 8. Behavior of invariants and error norms for $N = 262{,}144$, with $c = 0.03$, $\Delta t = 0.001$, $\Delta x = 0.1$, and varying t values for Example 3.4

	t	I_M	I_E	L_∞	L_2	RMS	Amplitude
Presented Method	4	2.109399452999	0.127301238624	6.1773×10^{-6}	2.838×10^{-5}	1.7527×10^{-7}	0.089999
RBF-PS [9]	4	2.1065191	0.1271746	1.9653×10^{-4}	2.3700×10^{-4}	-	-
RBF-FD [9]	4	2.1065191	0.1271746	1.9653×10^{-4}	2.3700×10^{-4}	-	-
[15]	4	2.1070945	0.1273011	2.3008×10^{-4}	4.1224×10^{-4}	-	-
[42]	4	2.10701	0.127301	2.2998×10^{-4}	4.1198×10^{-4}	-	-
Presented Method	8	2.109399452999	0.127301238620	1.7643×10^{-7}	8.208×10^{-7}	5.0693×10^{-9}	0.089999
RBF-PS [9]	8	2.1078906	0.1271752	2.9397×10^{-4}	5.3916×10^{-4}	-	-
RBF-FD [9]	8	2.1078906	0.1271752	2.9397×10^{-4}	5.3914×10^{-4}	-	-
[15]	8	2.1070945	0.1273011	2.2109×10^{-4}	5.1129×10^{-4}	-	-
[42]	8	2.10701	0.127301	2.2103×10^{-4}	5.1122×10^{-4}	-	-
Presented Method	12	2.109399452999	0.127301238626	6.3537×10^{-6}	2.920×10^{-5}	1.2674×10^{-8}	0.090000
RBF-PS [9]	12	2.1078906	0.1271752	3.4225×10^{-4}	8.4082×10^{-4}	-	-
RBF-FD [9]	12	2.1078906	0.1271752	3.4225×10^{-4}	8.4082×10^{-4}	-	-
[15]	12	2.1070945	0.1273011	2.1260×10^{-4}	5.3606×10^{-4}	-	-
[42]	12	2.10701	0.127301	2.1254×10^{-4}	5.3556×10^{-4}	-	-

Table 8. (cont.)

	t	I_M	I_E	L_∞	L_2	RMS	Amplitude
Presented Method	16	2.109399452999	0.127301238624	6.4424×10^{-6}	2.961×10^{-5}	1.2674×10^{-8}	0.089999
RBF-PS [9]	16	2.1100431	0.1271764	3.6616×10^{-4}	1.1028×10^{-3}	-	-
RBF-FD [9]	16	2.1100431	0.1271764	3.6616×10^{-4}	1.1028×10^{-3}	-	-
[15]	16	2.1070945	0.1273011	2.1388×10^{-4}	5.4486×10^{-4}	-	-
[42]	16	2.10701	0.127301	2.1388×10^{-4}	5.1387×10^{-4}	-	-
Presented Method	20	2.109399452999	0.127301238625	4.4249×10^{-7}	2.052×10^{-6}	1.2674×10^{-8}	0.089998
RBF-PS [9]	20	2.1113305	0.1272405	4.1865×10^{-4}	1.3340×10^{-3}	-	-
RBF-FD [9]	20	2.1113305	0.1272405	4.1865×10^{-4}	1.3340×10^{-3}	-	-
[15]	20	2.1045802	0.127301	4.3154×10^{-4}	5.6955×10^{-4}	-	-
[42]	20	2.10701	0.127301	4.3154×10^{-4}	5.6246×10^{-4}	-	-

3.5 *Generalized Rosenau-Regularized Long Wave (GN-R-RLW) equation*

Considering Eq. (5), the exact solution is given by [43], where the initial condition is obtained by setting $t = 0$.

$$u(x,t) = e^{\ln\left[\frac{(p+3)(3p+1)(p+1)}{2(p^2+3)(p^2+4p+7)}\right] \Big/ (p-1)} \cdot \operatorname{sech}^{\frac{4}{(p-1)}}\left[\frac{p-1}{\sqrt{4p^2+8p+20}}(x-ct)\right]. \tag{36}$$

Where $p \geq 2$ is an integer and $c = \frac{(p^4+4p^3+14p^2+20p+25)}{(p^4+4p^3+10p^2+12p+21)}$. In this example, the employed method's performance is evaluated for various values of the parameter p. Figure 5 displays the results of the wave motion, error vectors, and 3D visualizations for $p = 6$, 8, 16, 20 respectively. The wave motion verifies the conservation property of the method by showing that the amplitude stays nearly constant over the simulation. Table 9 presents the behavior of error norms and invariants at $t = 40$ for $p = 6$. The results show that as N increases, the error decreases and leads to a significantly improved accuracy, compared to the other methods. Furthermore, using a fixed $\Delta t = 0.001$ and $\Delta x = 0.1$, the behavior of invariants and error norms for $N = 262{,}144$ at various values t for $(p = 6, 8, 16, \text{and } 20)$ is shown in Table 10. The results demonstrate small error norms, verifying the accuracy and efficiency of the method across a variety of p values. For additional verification, we take $p = 20$, for the first time, providing a comprehensive examination of the method as the nonlinear term increases.

Table 9. Behavior of invariants and error norms at $t = 40$, $p = 6$, with $\Delta t = 0.001$, $\Delta x = 0.1$, and varying N values for Example 5

N	I_M	I_E	L_∞	L_2	Amplitude	CPU (s)
4,096	7.976598179339	3.834374089154	7.8268×10^{-1}	2.3402×10^{0}	0.744499	3.8787
8,192	7.977572122950	3.834809030332	3.9705×10^{-1}	1.1864×10^{0}	0.744560	7.8200
16,384	7.978059094756	3.835026503076	2.0434×10^{-1}	6.0982×10^{-1}	0.744590	16.1415
32,768	7.978302580659	3.835135239987	1.0805×10^{-1}	3.2204×10^{-1}	0.744606	35.6489
65,536	7.978424323611	3.835189608577	6.0074×10^{-2}	1.7902×10^{-1}	0.744615	74.0963
131,072	7.978485195086	3.835216792905	3.6897×10^{-2}	1.0873×10^{-1}	0.744620	168.3828
262,144	7.978515630824	3.835230385078	2.6761×10^{-2}	7.4908×10^{-2}	0.744622	365.0799
524,288	7.978530848693	3.835237181166	2.1804×10^{-2}	5.9002×10^{-2}	0.744623	728.4474

Table 10. Behavior of invariants and error norms for $N = 262{,}144$, $p = 6,\ 8,\ 16$, and 20 with $\Delta t = 0.001$, $\Delta x = 0.1$, and varying t values for Example 5

t	I_M	I_E	L_∞	L_2	RMS	Amplitude
			$\boldsymbol{p = 6}$			
10	7.978515630824	3.835230441100	1.1927×10^{-3}	3.5470×10^{-3}	2.1907×10^{-5}	0.744703
20	7.978515630824	3.835230385850	1.3705×10^{-5}	3.6582×10^{-5}	2.2594×10^{-7}	0.744620
30	7.978515630824	3.835230385122	2.0153×10^{-5}	5.5401×10^{-5}	3.4218×10^{-7}	0.744708
40	7.978515630824	3.835230385078	2.6761×10^{-5}	7.4908×10^{-5}	4.6265×10^{-7}	0.744622
			Comparative study with other methods at $t = 40$			
[44]	-	-	3.4181×10^{-4}	1.7187×10^{-3}	-	-
			$\boldsymbol{p = 8}$			
10	9.742059146351	4.735145581889	1.0679×10^{-3}	3.3513×10^{-3}	2.0699×10^{-5}	0.782277
20	9.742059146351	4.735145538670	1.1931×10^{-5}	3.3043×10^{-5}	2.0409×10^{-7}	0.782302
30	9.742059146351	4.735145536896	1.7785×10^{-5}	5.0653×10^{-5}	3.1285×10^{-7}	0.782251
40	9.742059146351	4.735145536917	2.3919×10^{-5}	6.9281×10^{-5}	4.2790×10^{-7}	0.782282
			Comparative study with other methods at $t = 40$			
[45]	9.742126	4.735346	1.3784×10^{-4}	3.8078×10^{-4}	-	-
[45]	9.742181	4.735225	2.9490×10^{-5}	7.5220×10^{-5}	-	-
[45]	9.742146	4.735302	6.2856×10^{-4}	1.7039×10^{-3}	-	-
[45]	9.742227	4.735082	4.7892×10^{-4}	1.2762×10^{-3}	-	-
[12]	-	-	1.5959×10^{-2}	3.1749×10^{-3}	-	-
[43]	-	-	1.6189×10^{-3}	4.3184×10^{-3}	-	-
			$\boldsymbol{p = 16}$			
10	17.156260476226	8.375295676554	7.3406×10^{-4}	2.7668×10^{-3}	1.7089×10^{-5}	0.853824
20	17.156260476226	8.375295655487	7.8200×10^{-6}	2.4897×10^{-5}	1.5377×10^{-7}	0.853813
30	17.156260476226	8.375295653900	1.1937×10^{-5}	3.8563×10^{-5}	2.3818×10^{-7}	0.853789
40	17.156260476226	8.375295653747	1.6464×10^{-5}	5.3419×10^{-5}	3.2993×10^{-7}	0.853825
			Comparative study with other methods at $t = 40$			
[45]	17.168699	8.375376	4.4109×10^{-4}	2.3334×10^{-3}	-	-
[45]	17.169258	8.375400	4.4493×10^{-4}	2.3199×10^{-3}	-	-
[45]	17.172776	8.375393	5.3860×10^{-4}	3.0231×10^{-3}	-	-
[45]	17.116828	8.375272	2.2709×10^{-3}	7.6218×10^{-3}	-	-
[43]	-	-	1.1875×10^{-3}	3.5725×10^{-3}	-	-
			$\boldsymbol{p = 20}$			
10	20.964963894268	10.235049699628	6.3458×10^{-4}	2.5696×10^{-3}	1.5870×10^{-5}	0.872546
20	20.964963894268	10.235049682475	6.6867×10^{-7}	2.2573×10^{-5}	1.3942×10^{-7}	0.872576
30	20.964963894268	10.235049681618	1.0259×10^{-5}	3.4935×10^{-5}	2.1577×10^{-7}	0.872586
40	20.964963894268	10.235049681404	1.4235×10^{-5}	4.8389×10^{-5}	2.9886×10^{-7}	0.872592

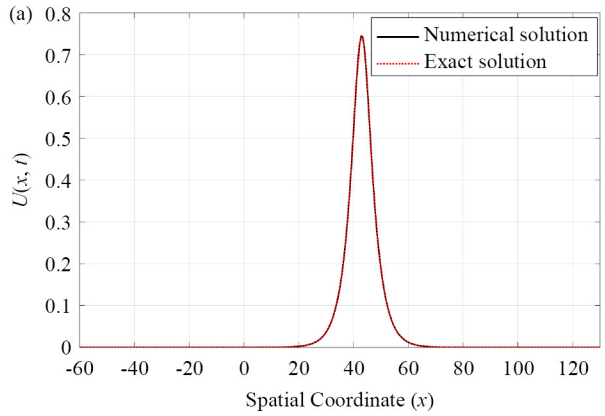
(a)
Numerical solution
Exact solution
U(x, t)
Spatial Coordinate (x)

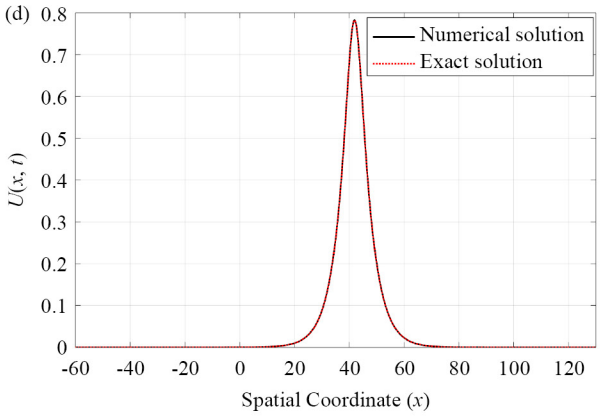
(d)
Numerical solution
Exact solution
U(x, t)
Spatial Coordinate (x)

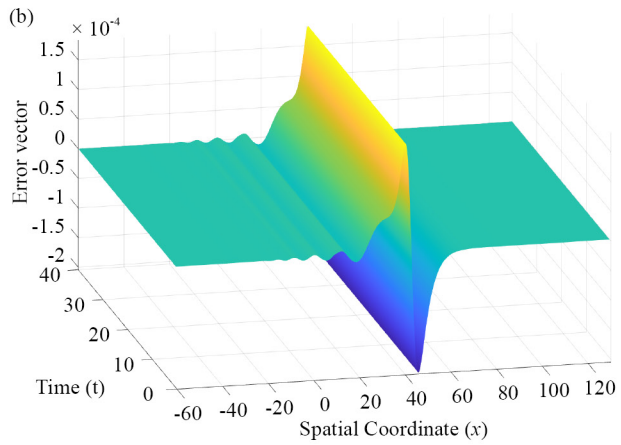
(b)
× 10^-4
Error vector
Time (t)
Spatial Coordinate (x)

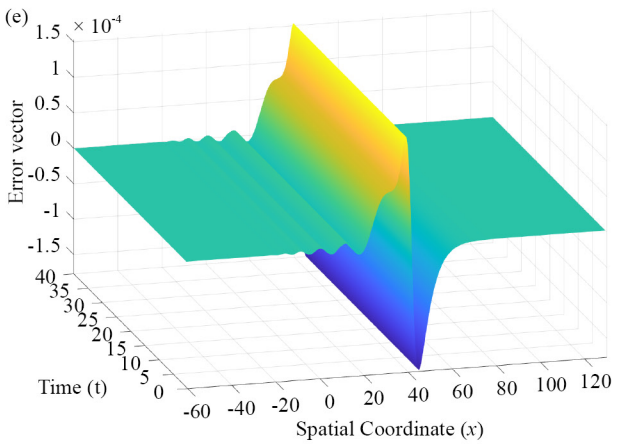
(e)
× 10^-4
Error vector
Time (t)
Spatial Coordinate (x)

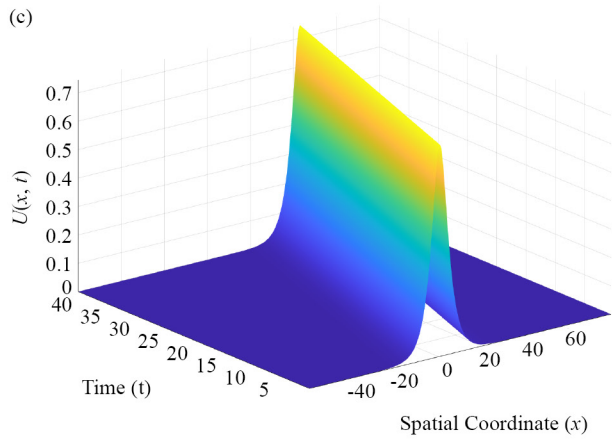
(c)
U(x, t)
Time (t)
Spatial Coordinate (x)

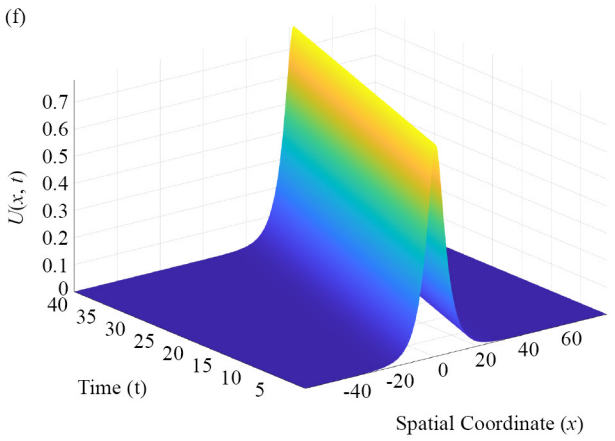
(f)
U(x, t)
Time (t)
Spatial Coordinate (x)

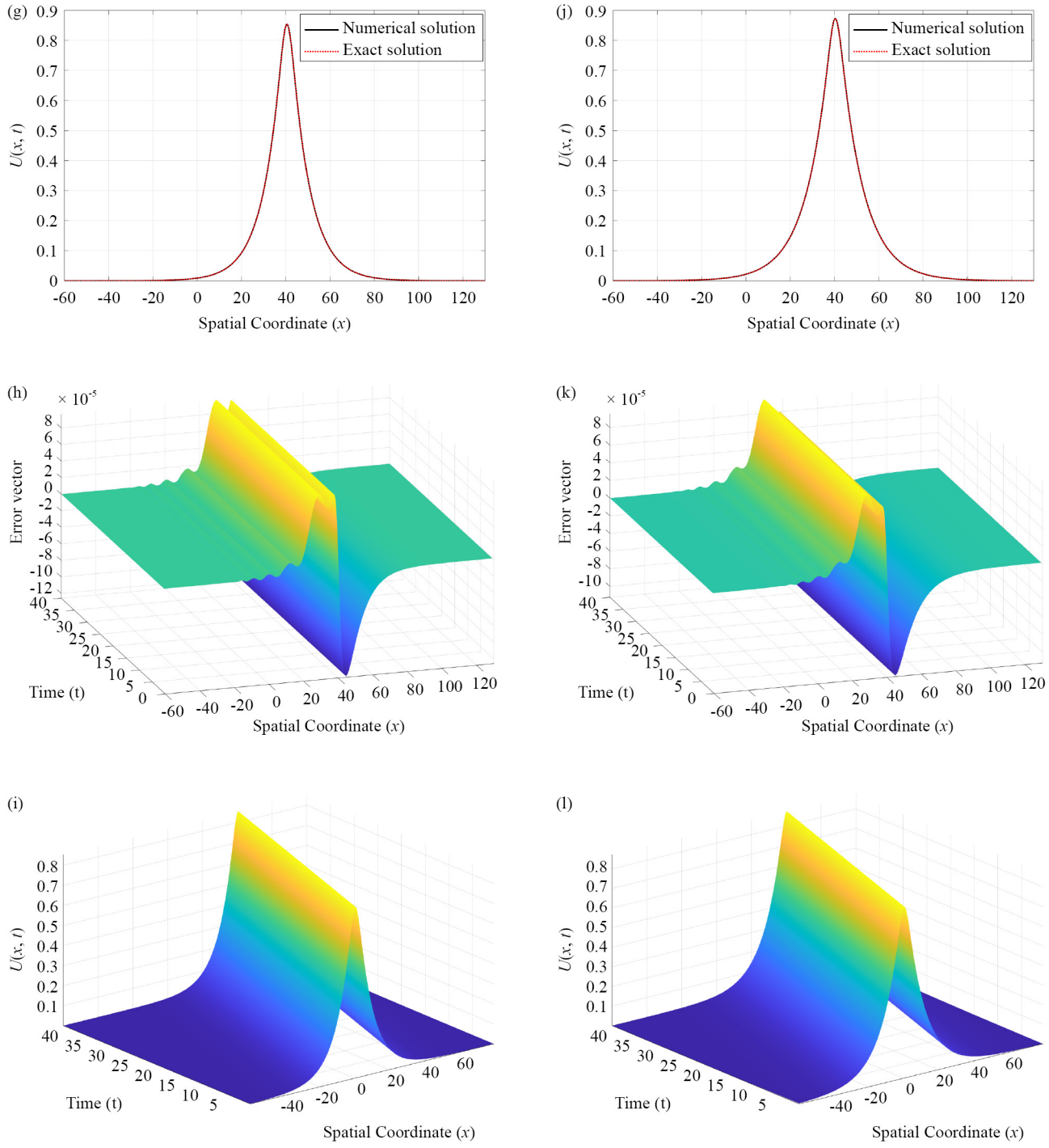

Figure 5. Visualization of the wave motion in Example 3.5 at $t = 40$, with $N = 16{,}384$, $\Delta t = 0.001$, and $\Delta x = 0.1$. (a), (d), (g), and (j) show the numerical and exact solutions for $p = 6,\ 8,\ 16,\ 20$, respectively. (b), (e), (h), and (k) show the corresponding error vectors. (c), (f), (i), and (l) present the 3D representations of the solitary wave

4. Conclusions

This article focused on solving nonlinear partial differential equations with initial conditions numerically. A computational method has been conducted using the Fourier spectral method for space and a central finite difference

method for time. The employed method was evaluated through error norms and conservation properties for various nonlinear equations to assess accuracy and efficiency, including the mFW equation, the mDP equation, the mCH equation, the KdV-BBM-B equation, and the GN-R-RLW equation. The results demonstrate that the proposed method preserves the momentum I_M and energy I_E invariants, while the L_2 and L_∞ errors decrease with finer spatial and temporal resolutions, achieving high accuracy and maintaining the solitary wave amplitude and shape during propagation. Additionally, the method provides a reliable numerical framework that can be extended to model real-world nonlinear PDEs in fluid mechanics, plasma physics, and materials science.

Acknowledgement

The authors are grateful to the referees and the editor for carefully checking the details and for helpful comments that improved this paper.

Conflict of interest

The authors declare no competing financial interest.

References

[1] Alharthi M. The modulations of collapsing stochastic (2 + 1)-dimensional Maccari system structures. *Alexandria Engineering Journal*. 2025; 129: 738-743.

[2] Zeidan D, Pradhan PK, Pandey M. Similarity solutions and wave interactions in a rarefied polyatomic gas. *International Journal of Engineering Science*. 2025; 212: 104262.

[3] Miah SS, Akar MA, Khan K. Solitary wave solutions with stability, bifurcation, sensitivity and chaotic analysis of the (3 + 1)-dimensional Yu-Toda-Sasa-Fukuyama equation using beta derivative. *Partial Differential Equations in Applied Mathematics*. 2025; 14: 101192.

[4] He B, Meng Q, Li S. Explicit peakon and solitary wave solutions for the modified Fornberg–Whitham equation. *Applied Mathematics and Computation*. 2010; 217(5): 1976-1982.

[5] Çelikkaya İ. Travelling peakon and solitary wave solutions of modified Fornberg–Whitham equations with nonhomogeneous boundary conditions. *International Journal of Nonlinear Sciences and Numerical Simulation*. 2023; 24(2): 661-671.

[6] Celikkaya I. A novel numerical simulations for Fornberg–Whitham and modified Fornberg–Whitham equations with nonhomogeneous boundary conditions. *Journal of Nonlinear Modeling and Analysis*. 2024; 6(2): 273-287.

[7] Nisar KS. A constructive numerical approach to solve the fractional modified Camassa–Holm equation. *Alexandria Engineering Journal*. 2024; 106: 19-24.

[8] Wazwaz AM. Solitary wave solutions for modified forms of Degasperis–Procesi and Camassa–Holm equations. *Physics Letters A*. 2006; 352(6): 500-504.

[9] Nikan O, Golbabai A, Nikazad T. Solitary wave solution of the nonlinear KdV-Benjamin-Bona-Mahony-Burgers model via two meshless methods. *The European Physical Journal Plus*. 2019; 134: 1-14.

[10] Alrzqi SF, Alrawajeh FA, Hassan HN. An efficient numerical technique for investigating the generalized Rosenau–KDV–RLW equation by using the Fourier spectral method. *AIMS Mathematics*. 2024; 9(4): 8661-8688.

[11] Shaheen S, Haq S, Ghafoor A. A meshfree technique for the numerical solutions of nonlinear Fornberg–Whitham and Degasperis–Procesi equations with their modified forms. *Computational and Applied Mathematics*. 2022; 41(4): 183.

[12] Verma AK, Rawani MK. Numerical solutions of generalized Rosenau–KDV–RLW equation by using Haar wavelet collocation approach coupled with nonstandard finite difference scheme and quasilinearization. *Numerical Methods for Partial Differential Equations*. 2023; 39(2): 1085-1107.

[13] Çelik İ. Jacobi wavelet collocation method for the modified Camassa–Holm and Degasperis–Procesi equations. *Engineering with Computers*. 2022; 38(3): 2271-2287.
[14] Chand A, Mohapatra J. Local discontinuous Galerkin finite element method for the nonlinear Korteweg–de Vries-Benjamin-Bona-Mahony-Burgers equation. *Physics of Fluids*. 2025; 37(3): 037149.
[15] Karakoc SBG, Bhowmik SK. Galerkin finite element solution for Benjamin–Bona–Mahony–Burgers equation with cubic B-splines. *Computers & Mathematics with Applications*. 2019; 77(7): 1917-1932.
[16] Yamazaki Y, Harandi A, Muramatsu M, Viardin A, Apel M, Brepols T, et al. A finite element-based physics-informed operator learning framework for spatiotemporal partial differential equations on arbitrary domains. *Engineering with Computers*. 2025; 41(1): 1-29.
[17] Li S, Liu J. The Legendre Galerkin spectral element method for the generalized Rosenau-type equations. *Journal of Applied Mathematics and Computing*. 2025; 71: 3059-3086.
[18] Jiang W, Gao X. Review of collocation methods and applications in solving science and engineering problems. *Computer Modeling in Engineering & Sciences (CMES)*. 2024; 140(1): 41.
[19] Abd-Elhameed WM, Al-Harbi MS, Amin AK, Ahmed HM. Spectral treatment of high-order Emden–Fowler equations based on modified Chebyshev polynomials. *Axioms*. 2023; 12(2): 99.
[20] Weera W, Kumar RV, Sowmya G, Khan U, Prasannakumara B, Mahmoud EE, et al. Convective-radiative thermal investigation of a porous dovetail fin using spectral collocation method. *Ain Shams Engineering Journal*. 2023; 14(1): 101811.
[21] Kamran, Shah FA, Shah K, Abdeljawad T. Numerical solution of two dimensional time-fractional telegraph equation using Chebyshev spectral collocation method. *Partial Differential Equations in Applied Mathematics*. 2025; 13: 101129.
[22] Wang W, Zhang H, Zhou Z, Yang X. A fast compact finite difference scheme for the fourth-order diffusion-wave equation. *International Journal of Computer Mathematics*. 2024; 101: 170-193.
[23] Kapoor M. A comparative study of numerical simulations via UAT and UAH tension B-splines for coupled Navier–Stokes equation with statistical validation. *Partial Differential Equations in Applied Mathematics*. 2025; 13: 101127.
[24] Xu Q, Wang Y. Spatial filter for the pseudo-spectral implementation of fractional derivative wave equation. *Pure and Applied Geophysics*. 2022; 179(8): 2831-2840.
[25] Lyu Y, Li X. RBF-based quasi-interpolating pseudo-spectral method for solving nonlinear dispersive PDEs. *Aerospace Systems*. 2025. Available from: https://doi.org/10.1007/s42401-025-00394-6.
[26] Wang X, Wang J, Wang X, Yu C. A pseudo-spectral Fourier collocation method for inhomogeneous elliptical inclusions with partial differential equations. *Mathematics*. 2022; 10(3): 296.
[27] Cheng Y, Wang T. Convergence study of two exponential wave integrator Fourier pseudo-spectral methods for the nonlinear Schrödinger equation with wave operator. *Calcolo*. 2025; 62(1): 1-36.
[28] Zhang Q, Yan T, Xu D, Chen Y. Direct/split invariant-preserving Fourier pseudo-spectral methods for the rotation-two-component Camassa–Holm system with peakon solitons. *Computer Physics Communications*. 2024; 302: 109237.
[29] Abdelkader L. An effective operational matrix method for the solution of non-linear third-order initial value problems. *International Journal of Applied Mathematics and Simulation*. 2025; 2(1): 50-61.
[30] Kumar S, Gupta V, Zeidan D. An efficient collocation technique based on operational matrix of fractional-order Lagrange polynomials for solving the space-time fractional-order partial differential equations. *Applied Numerical Mathematics*. 2024; 204: 249-264.
[31] Gong Y, Hong Q, Wang Q. Supplementary variable method for thermodynamically consistent partial differential equations. *Computer Methods in Applied Mechanics and Engineering*. 2021; 381: 113746.
[32] Youssri YH, Abd-Elhameed WM, Elmasry AA, Atta AG. An efficient Petrov–Galerkin scheme for the Euler–Bernoulli beam equation via second-kind Chebyshev polynomials. *Fractal and Fractional*. 2025; 9(2): 78.
[33] Shang Y, Wang F, Sun J. Randomized neural network with Petrov–Galerkin methods for solving linear and nonlinear partial differential equations. *Communications in Nonlinear Science and Numerical Simulation*. 2023; 127: 107518.
[34] Rasekhinezhad H, Abbasbandy S, Allahviranloo T, Babolian E. A reproducing kernel method for solving nonlocal functional differential equations with delayed or advanced arguments. *Computational Methods for Differential Equations*. 2025; 14(1): 1-13.
[35] Sun Z, Ling L. A kernel-based meshless conservative Galerkin method for solving Hamiltonian wave equations. *SIAM Journal on Scientific Computing*. 2022; 44(4): A2789-A2807.

[36] Esfahani A. Solitary wave solutions for generalized Rosenau-KdV equation. *Communications in Theoretical Physics*. 2011; 55(3): 396-398.

[37] Pandit S, Jiwari R, Bedi K, Koksal ME. Haar wavelets operational matrix based algorithm for computational modelling of hyperbolic type wave equations. *Engineering Computations*. 2017; 34(8): 2793-2814.

[38] Harris AP, Biala TA, Khaliq AQ. Fourier spectral methods with exponential time differencing for space-fractional partial differential equations in population dynamics. *Numerical Methods for Partial Differential Equations*. 2023; 39(4): 2963-2974.

[39] Hassan HN, Saleh HK. Fourier spectral methods for solving some nonlinear partial differential equations. *International Journal of Open Problems in Computer Mathematics*. 2013; 6(2): 144-179.

[40] Hassan HN. An efficient numerical method for the modified regularized long wave equation using Fourier spectral method. *Journal of the Association of Arab Universities for Basic and Applied Sciences*. 2017; 24: 198-205.

[41] Wazwaz AM. New solitary wave solutions to the modified forms of Degasperis–Procesi and Camassa–Holm equations. *Applied Mathematics and Computation*. 2007; 186(1): 130-141.

[42] Driscoll TA, Fornberg B. Interpolation in the limit of increasingly flat radial basis functions. *Computers & Mathematics with Applications*. 2002; 43(3-5): 413-422.

[43] Wongsaijai B, Poochinapan K, Disyadej T. A compact finite difference method for solving the general Rosenau–RLW equation. *IAENG International Journal of Applied Mathematics*. 2014; 44(4). Available from: https://www.researchgate.net/profile/Ben-Wongsaijai/publication/274082789.

[44] Mittal R, Jain R. Numerical solution of general Rosenau-RLW equation using quintic B-splines collocation method. *Communications in Numerical Analysis*. 2012; 2012: 1-16.

[45] Arı M, Dereli Y. Numerical solutions of the general Rosenau–RLW equation using meshless kernel based method of lines. *Journal of Physics: Conference Series*. 2016; 766(1): 012030.